

Two stages in three-dimensional *in vitro* growth of tissue generated by osteoblastlike cells

Krishna P. Kommareddy and Claudia Lange

Department of Biomaterials, Max Planck Institute of Colloids and Interfaces, 14424 Potsdam, Germany

Monika Rimpler

Ludwig Boltzmann Institute of Osteology at the Hanusch Hospital of WGKK and AUVA Trauma Centre Meidling, 4th Medical Department, Hanusch Hospital, Vienna, Austria

John W. C. Dunlop and Inderchand Manjubala

Department of Biomaterials, Max Planck Institute of Colloids and Interfaces, 14424 Potsdam, Germany

Jing Cui, Karl Kratz, and Andreas Lendlein

Center for Biomaterial Development, Institute of Polymer Research, GKSS Research Center Geesthacht GmbH and Berlin-Brandenburg-Center for Regenerative Therapies (BCRT), Kantstrasse 55, 14513 Teltow, Germany

Peter Fratzl^{a)}

Department of Biomaterials, Max Planck Institute of Colloids and Interfaces, 14424 Potsdam, Germany

(Received 1 April 2010; accepted 27 April 2010; published 2 June 2010)

Bone regeneration is controlled by a variety of biochemical, biomechanical, cellular, and hormonal mechanisms. In particular, physical properties of the substrate such as stiffness and architecture highly influence the proliferation and differentiation of cells. The aim of this work is to understand the influence of scaffold stiffness and cell seeding densities on the formation of tissue by osteoblast cells within polyether urethane scaffolds containing pores of different sizes. MC3T3-E1 preosteoblast cells were seeded on the scaffold, and the amount of tissue formed within the pores was analyzed for culture times up to 49 days by phase contrast microscopy. The authors show that the kinetics of three-dimensional tissue growth in these scaffolds follows two stages and can be described by a universal growth law. The first stage is dominated by cell-material interactions with cell adherence and differentiation being strongly dependent on the polymer material. After a delay time of a few weeks, cells begin to grow within their own matrix, the delay being strongly dependent on substrate stiffness and seeding protocols. In this later stage of growth, three-dimensional tissue amplification is controlled rather by the pore geometry than the scaffold material properties. This emphasizes how geometric constraints may guide tissue formation *in vitro* and shows that optimizing scaffold architectures may improve tissue formation independent of the scaffold material used. © 2010 American Vacuum Society. [DOI: 10.1116/1.3431524]

I. INTRODUCTION

Porous three-dimensional (3D) scaffolds with interconnected pore channels are used extensively in the field of bone tissue engineering.^{1,2} The interconnected pore channel network and pore architecture allows cells to penetrate into the scaffold and be supplied with nutrients, enhancing new tissue growth by the cells.^{3,4} Previous reports have shown that a variety of physical parameters of the scaffold influences the behavior of osteoblast cells, specifically the local surface chemistry,^{5,6} physical characteristics such as material topography,⁷⁻⁹ roughness,^{10,11} as well as stiffness.¹²⁻¹⁴ The mechanical properties of the substrate, namely, stiffness, influence cell differentiation and proliferation.¹² Mesenchymal stem cells, for example, were shown to differentiate into neurogenic lineages on soft substrates (0.1–1 kPa), myogenic lineages on stiffer substrates (8–17 kPa), and osteogenic lineages on relatively rigid substrates (25–40 kPa).¹⁵ It has also

been demonstrated that cell adhesion depends on roughness and the nanostructure of the surface¹⁶⁻²⁰ with a higher differentiation potential and lower proliferation rate being observed on rougher surfaces.¹⁶ In addition to geometric features at the nanoscale, the topology of the local environment, at length scales larger than the cell size, also affects the behavior of cells.⁹ These larger length scales, such as the pore size of scaffolds, significantly influence cell adhesion, migration, and growth,²¹⁻²³ but the extent of tissue formation by the cells in these pore channels has been rarely studied.

In our earlier study, we designed a simple model system to investigate the effect of pore shape and size within hydroxyapatite (HA) scaffolds (stiffness in the gigapascal range) on the tissue formation by murine preosteoblast cells.²⁴ In the initial phase of tissue formation in the scaffold, cells migrate, adhere, and proliferate within the pore structure, a process which is strongly influenced by the material properties, and later with ongoing culture time, cells synthesize sufficient amounts of matrix to proliferate inside their own extracellular matrix.^{25,26} In the present study we want to

^{a)}Author to whom correspondence should be addressed; electronic mail: fratzl@mpikg.mpg.de

explore whether pure polymer substrates with different stiffnesses can influence the tissue growth kinetics. The polymers were selected such that the mechanical properties of the model scaffolds remained constant during the cell culture experiment. We selected a polyether urethane (PU) with adjustable stiffness in the megapascal range (that is, lower than HA) as the polymer matrix to produce scaffolds with different pore sizes and shapes, which are stable under physiological conditions. Such PU polymers exhibited good cell compatibility in *in vitro* tests^{27,28} and biocompatibility in *in vivo* studies as artificial heart valve and wound dressings²⁹ or as a potential dialysis catheter.³⁰ The scaffold stiffnesses were controlled by modifying the multiblock copolymer segment ratio of the PU.^{31,32} These materials also have the potential for the creation of a thermally induced shape-memory effect, which could be useful for future applications with changeable pore sizes.^{33,34} Cell culture experiments were performed on the scaffolds using MC3T3-E1 preosteoblast cells, a well established cell line for bone biology studies^{35–37} known for lineage differentiation into mature osteoblasts. These experiments enabled the influence of stiffness and different cell seeding protocols on the kinetics of tissue formation to be investigated and compared to the results from the earlier HA scaffolds.²⁴

II. MATERIALS AND METHODS

A. Materials

Aliphatic polyether urethanes (PU) supplied by Noveon (Wilmington, MA) with the trade name Tecoflex[®] were used directly without further purification. The mechanical properties of the polymer sheets were determined from tensile tests at ambient temperature and at 37 °C in water. Tensile tests were carried out on a Z005 tensile tester (Zwick, Ulm, Germany) at ambient temperature and on a Z1.0 tensile tester equipped with a temperature controlled liquid chamber at 37 °C in water, with a strain rate of 5 mm/min. For each PU composition five measurements were conducted. The selected polymer samples are named PU75, PU120, and PU310 according to their elastic modulus (E-Modulus) determined at ambient temperature. Furthermore dynamic mechanical analysis at varied temperature (DMTA) measurements were performed on an Eplexor[®] 25 N (Gabo, Ahlden, Germany) to follow the changes in thermomechanical properties when the polymer specimen [type DIN EN ISO 1BB ($I_0=20$ mm, width=2 mm, and thickness=2 mm)] was stored for 1 h, 5 h, 1 d, 3 d, 7 d, and 14 d in cell culture medium.

B. Scaffold processing

HAAKE Minijet-Micro injection molding machine (Thermo Electron GmbH, Karlsruhe, Germany) was applied to prepare 2 mm thick polymer scaffolds with square-shaped pores. The mold temperature was maintained at 25 °C with a pressure of 8 bars. The extrusion cylinder temperatures were 190 °C for PU75, 200 °C for PU120, and 210 °C for PU310. Three different pore sizes were produced in the scaffold.

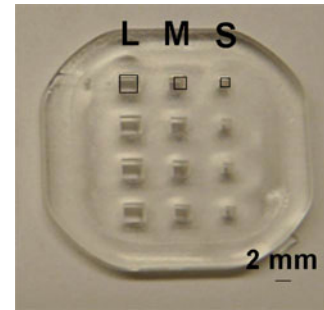


FIG. 1. (Color online) Representative image of PU120 scaffolds with square pores of different perimeters (p). S: $p=3.14$ mm, M: $p=4.71$ mm, and L: $p=6.28$ mm. The thickness of the scaffolds is 2 mm.

fold. The perimeters of the small, middle, and large pores were 3.14, 4.71, and 6.28 mm, respectively (Fig. 1).

C. Surface characterization

Surface profiles of the 3D injection molded scaffolds were obtained with an optical profilometer type MicoProf 200 equipped with a CWL 300 (Fries Research & Technology GmbH) chromatic white-light sensor. The measurements were performed on the cell contact surface in between the pores. Data acquisition was performed with the software AQUIRE (ver. 1.21), while the evaluation was completed with software MARK III (ver. 3.8b). The lateral resolution was 1–2 μm and ~ 5 nm in the z -direction. The surface profile and the roughness (R_q) were analyzed. Three scans were conducted at different scanning areas of $50 \times 50 \mu\text{m}^2$. The points and lines were 2000×2000 and the acquisition rate was 300 Hz.

The wettability of the PU was determined by dynamic contact angle (CA) measurements using the captive bubble method. The injection molded two-dimensional (2D) test specimens (diameter=15 mm, thickness=2 mm, and $R_q = 5 \pm 1 \mu\text{m}$) were equilibrated in water for 30 min before starting the measurement. The diameter of the contact area between the surface and the bubble was around 2 mm. Advancing and receding contact angle measurements were performed by stepwise withdrawing/adding of air from/to the captured bubble. CA measurements were realized at ambient temperature with a DSA 100 (KRÜSS, Hamburg, Germany). At least ten measurements on three different locations were performed and averaged to yield the contact angles and their standard deviation.

For investigation of changes in surface properties during cell culture procedures the surface roughness of the scaffolds and the contact angle of 2D samples were measured after storage in α -modification minimum essential medium (α -MEM) (Sigma-Aldrich, Steinheim, Germany) for 3 h at 37 °C.

D. Cell culture experiments

The preosteoblastic mouse calvariae MC3T3-E1 cell line (generous gift from Dr. F. Varga, Ludwig Boltzmann Institute of Osteology, Vienna, Austria) was used for *in vitro* experi-

ments. For seeding on scaffolds, near confluent cells during fourth passage treated with Pronase (Roche diagnostics GmbH, Mannheim, Germany) and ethylene diamine tetra acetate (EDTA) (Sigma-Aldrich, St. Louis, MO) were used. These cells were suspended in a culture medium of α -MEM (Sigma-Aldrich, St. Louis, MO) supplemented with 10% fetal calf serum (PAA laboratories, Linz, Austria), 50 $\mu\text{g}/\text{ml}$ ascorbic acid (Sigma-Aldrich, St. Louis, MO), and 30 $\mu\text{g}/\text{ml}$ gentamicin (Sigma-Aldrich, Steinheim, Germany). The cell seeded scaffolds were incubated in a humidified atmosphere with 5% CO_2 at 37 °C up to 49 days, while changing the medium twice a week. Three different cell seeding protocols were followed in cell culture experiments. In the first protocol, 1×10^5 cells/ cm^2 were suspended in 3 ml of medium and poured onto the scaffolds. In the second protocol, 3×10^5 cells/ cm^2 were suspended in 3 ml of medium and poured on the scaffolds with square pores. In both protocols, the cells initially attach on the surface of the scaffold and then migrate into the pores. In the third protocol, 8×10^4 cells/ cm^2 were suspended in a minimal amount of medium and dropped on surface of the scaffold with square pores, leading to aspiration of cell suspension by the pores, which enables complete covering of pores with cells from the very beginning. The second two seeding protocols were performed twice under identical conditions, and the first protocol was performed once only.

E. DAPI staining and visualization of cell shape

To analyze the initial cell attachment on the surface of PU scaffolds, about 1×10^5 cells/ cm^2 were suspended in medium and seeded on the scaffolds. Initial cell attachment and distribution on the surface, after 6 h of incubation, were studied by 4', 6-diamidino-2'-phenylindole dihydrochloride (DAPI) staining (Roche diagnostics GmbH, Mannheim, Germany). After 6 h, the cell culture medium was removed and the cells were washed with DAPI-methanol solution (1 $\mu\text{g}/\text{ml}$) and incubated in fresh DAPI-methanol solution for 15 min at 37 °C. The staining solution was removed and the samples were washed in phosphate buffered saline (PBS) and observed under a fluorescence microscope (Leica DMRB, Wetzlar, Germany).

The cell shapes were visualized using DAPI-fluorescent isothiocyanate (FITC) staining. After 6 h, cells were briefly washed twice with PBS, and fixed in a 4% paraformaldehyde (PFA) (Fluka, Steinheim, Germany) solution for 15 min at room temperature. Unreacted PFA was washed off with PBS. Cells were then permeabilized with 0.1% Triton-X100 (Sigma-Aldrich, Steinheim, Germany) for 2 min, PBS washed, and stained with phalloidin-FITC (Invitrogen, Eugene, OR) for 1 h. Later samples were washed several times with PBS and stained with DAPI for 15 min at 37 °C. Finally the samples were washed in PBS and observed using a fluorescence microscope (Leica DM RXA2, Wetzlar, Germany) with an oil immersion objective and appropriate filters.

F. Alkaline phosphatase staining

The MC3T3-E1 osteoblastlike cells have the potential to undergo differentiation into mature osteoblasts.³⁵ Alkaline phosphatase (ALP) activity is an early differentiation marker of preosteoblastic cells to mature osteoblasts. After 21 days of culture, localization of ALP activity was qualitatively performed with the azo-dye method.³⁸ The cells were fixed in 4% PFA in PBS for 10 min, intensively rinsed with PBS, and then with 0.9% w/v NaCl (Roth, Karlsruhe, Germany). Afterwards the cells were incubated at 37 °C with naphthol AS-MX phosphate disodium salt (Sigma-Aldrich, St. Louis, MO) and fast blue RR salt (Sigma-Aldrich, Steinheim, Germany) in 5% sodium tetraborate (Sigma-Aldrich, Steinheim, Germany) buffer containing 0.9% NaCl and MgSO_4 (Sigma-Aldrich, Steinheim, Germany). Later the samples were placed in PBS and observed under an optical microscope in transmission mode (Leica DM RXA2, Wetzlar, Germany).

G. Confocal microscopy

The alignment of the cells and actin cytoskeleton in the newly formed three-dimensional tissue network was investigated with a confocal laser scanning microscope (Leica TCS SP, Heidelberg, Germany), 488 nm laser excitation was used, and emission measured at 514 nm. Cells were fixed in 4% PFA in PBS for 10 min, permeabilized with 0.1% Triton-X100 (Sigma-Aldrich, Steinheim, Germany), and later stained with FITC-conjugated-phalloidin ($4 \times 10^{-6} \text{M}$, Sigma-Aldrich, Steinheim, Germany) for 30 min at 4 °C.

H. Phase contrast microscopy and analysis of tissue formation

An inverted phase contrast microscope (Nikon Eclipse TS100 F, Düsseldorf, Germany) was used to monitor the cell distribution and tissue formation within the pores. Images were captured at least once a week over the culture period of 49 days. The amount of tissue formed within the pores by the cells was estimated from the projected tissue area as seen in the phase contrast images.²⁴ This projected tissue area was calculated from the area between the inner tissue-medium boundary and the original pore boundary imaged at the start of the experiment. This calculation was performed using IMAGE J software (NIH Image analysis software, Bethesda, MD).

I. Statistical analysis

The delay times (t_0) of tissue formation in all the experiments were analyzed for statistical significance using three way analysis of variance (ANOVA), performed to compare the interdependency of pore size, material, and seeding methods. All pairwise multiple comparisons were done by the Holm-Sidak method and p values of less than 0.05 were considered significant.

TABLE I. Mechanical properties of PU polymer materials determined by tensile tests.

Sample	E-Modulus at RT (MPa)	E-Modulus at 37 °C (MPa)
PU310	312 ± 53	208 ± 29
PU120	120 ± 27	7 ± 2
PU75	74 ± 7	6 ± 3

III. RESULTS

A. Scaffold properties

The PU polymers used were aliphatic multiblock copolymers synthesized from methylene bis(*p*-cyclohexyl isocyanate) ($H_{12}MDI$), poly(tetramethylene glycol) (PTMEG) ($M_n = 1000 \text{ g mol}^{-1}$), and 1,4-butanediol (1,4-BD).^{31,32} The thermal and mechanical properties of these PU polymers can be adjusted by variation of $H_{12}MDI/1,4-BD$ to $H_{12}MDI/PTMEG$ segment ratio. The composition, i.e., $H_{12}MDI/1,4-BD$ to $H_{12}MDI/PTMEG$ segment ratio analyzed by 1H -NMR spectroscopy, showed that for PU310 a $H_{12}MDI/1,4-BD$ segment content was about 58 wt % while the values for the PU120 and PU75 were around 45 wt %.³² Mechanical properties of the PU materials were investigated by tensile tests at ambient temperature, as well as under physiological conditions at 37 °C in water (Table I). The elastic modulus was found to increase with increasing content of $H_{12}MDI/1,4-BD$ segment from 75 to 310 MPa at ambient temperature. In addition, the mechanical properties explored under physiological conditions showed that all PU samples are significantly softer than at ambient temperature. For PU310 an elastic modulus of 208 MPa was observed, while PU120 and PU75 exhibited lower values around 6–7 MPa. The softening of the PU samples in water at 37 °C can be explained by approaching the temperature of the glass transition associated with the mixed phase in combination with a softening effect induced by a water uptake of 2 wt %. DMTA results obtained for samples stored in a cell culture medium over a time period of up to 14 d confirmed that the tensile mechanical properties in water at 37 °C remained unchanged, suggesting that the stiffness of the PUs is unlikely to change over the cell culture time period of 49 days.

The surface roughness of the PUs was explored on the cell contact area in between the pores. In the dry state the scaffolds prepared from PU310 and PU75 exhibited a surface roughness with $R_q = 110 \pm 20 \mu\text{m}$, which is in the range of the surface roughness of the mold. In contrast significant lower values were observed for PU120 with $R_q = 60 \pm 10 \mu\text{m}$, which we attribute to the different processing behaviors of the PU120 and PU75. However, the surface topology was not influenced by the immersion into cell culture medium for 3 h and the R_q values remained almost constant. The surface wettability was investigated for 2D samples by determination of contact angle. In these experiments we observed similar values for the advancing contact angle of the soft PUs (PU75 and PU120) around $\theta_{advancing}$

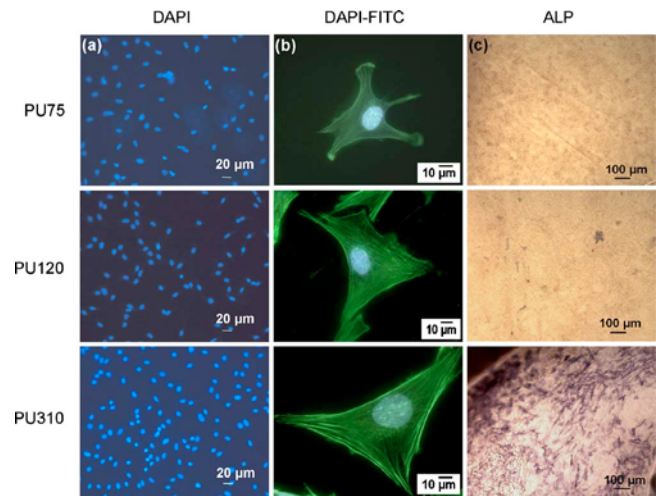


FIG. 2. (Color online) (a) DAPI staining of cells (nuclei) seeded at 10^5 cells/cm², 6 h after cell seeding (scale 20 μm). (b) FITC-DAPI staining of MC3T3-E1 cells showing the cytoskeleton and nucleus on PU75, PU120, and PU310, respectively (scale 10 μm). (c) Alkaline phosphatase enzyme staining of PU75, PU120, and PU310, respectively, after 21 days of culture (scale 100 μm).

$\approx 112^\circ$, while for PU310 a lower $\theta_{advancing} \approx 94^\circ$ was obtained. All PUs show a moderate hysteresis between advancing and receding angles of about 5° – 14° , indicating an almost homogeneous surface. After exposure to cell culture medium for 3 h at 37 °C nearly identical contact angles with $\theta_{advancing} \approx 110^\circ$ and $\theta_{hysteresis} \approx 16^\circ$ were achieved for all polymers.

B. Cell adhesion and cell shape

Adhesion of MC3T3-E1 preosteoblast cells on the surface of PU scaffolds was studied in terms of adhered number of cells and cell shape. On the polymer scaffold made from PU75, the softest polymer substrate used, a smaller number of cells were seen to adhere compared with PU120 and PU310 [Fig. 2(a)]. The individual cells observed by FITC staining showed many broad lamellipodia structures with less actin organization on PU75 with a smaller cell size [Fig. 2(b)]. Whereas on PU310 scaffolds, the stiffest polymer substrate used, the cells developed highly directional lamellipodia with more actin organization, formation of stress fibers, and cells were stretched more.

C. Alkaline phosphatase enzyme activity

Alkaline phosphatase is an early marker for differentiation of preosteoblasts to mature osteoblasts. The ALP activity of the cells was observed on the surface of the scaffolds, and positive cells showed a violet coloration. By comparing the ALP pattern on the three substrate, cells on PU310 exhibit a strong staining for ALP, whereas cells on the other two polymers, PU120 and PU75, were negative [Fig. 2(c)]. This suggests that the stiffer polymer substrate supports differentiation of osteoblast precursor cells.

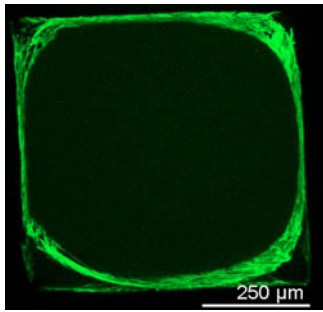


FIG. 3. (Color online) Two-dimensional stack projections of FITC-phalloidin staining of actin filaments in a small square pore of PU120 scaffolds after 49 days of culture (*z*-stack projection is 100 μm thick consisting of 100 sections with a 1 μm step size).

D. Confocal microscopy

The confocal microscope images of the pores after 49 days of culture showed that cells adhered to the surface of the scaffold after seeding and migration into the pores. Within the pores they proliferated and formed a tissuelike network. In the square pores cells predominantly started to proliferate in corner regions, as shown in Fig. 3. Within this tissuelike network cells built multilayers and actin-stress fibers of the cells in the tissue were aligned parallel to the internal tissue-medium border.

E. Tissue formation

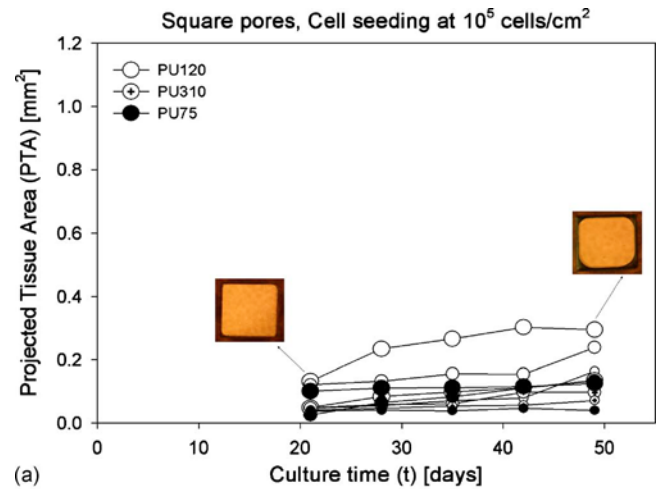
The amount of tissue formed in the pores was analyzed from phase contrast microscopy images. At a seeding concentration of 10^5 cells/ cm^2 , only limited tissue growth was observed making it difficult to distinguish between the effects of the different scaffold materials [Fig. 4(a)]. At a seeding density of 3×10^5 cells/ cm^2 , where the cells are confluent on the scaffolds after the initial cell attachment phase, the tissue growth rate was independent of channel size; however, tissue growth begins earlier for the highest scaffold stiffnesses [Fig. 4(b)]. For the experiments, in which cells are aspirated into the channels (8×10^4 cells/ cm^2), neither the substrate nor the channel size influenced the start of tissue growth although larger amounts of tissue were formed in the large pores compared to the smaller pores [Fig. 4(c)].

F. Tissue growth kinetics

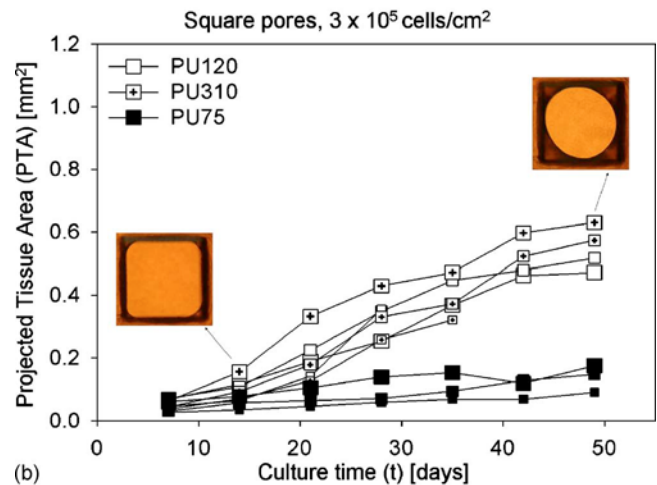
The tissue growth kinetics were analyzed using the same procedure reported for tissue growth on HA scaffolds, by determining the projected tissue area as a function of time within each pore.²⁴ The tissue growth in terms of projected tissue area A can be described in the form

$$A = K(t - t_0), \quad (1)$$

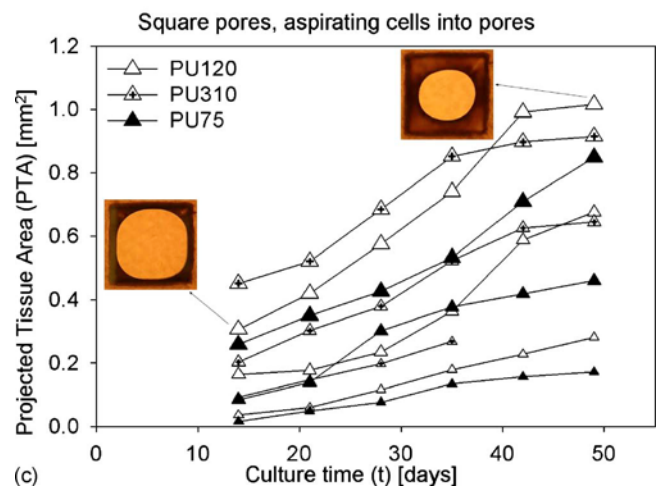
where K is the growth rate in the later stages and t_0 is the delay time needed to reach this stage of tissue growth. The delay time (t_0) was determined empirically by shifting the tissue area data (initially plotted as a function of culture time t) along the horizontal axis until the graphs nearly coincided, as shown in Fig. 5(a). Figure 5(b) summarizes all the data



(a)



(b)



(c)

FIG. 4. (Color online) Exemplary data of measured projected tissue area formed as a function of time tissue growth experiment made using different cell seeding protocols: (a) 10^5 cells/ cm^2 , (b) 3×10^5 cells/ cm^2 , and (c) aspiration of cells into pores. The symbols indicate the PU polymer used, PU75 (black), PU120 (white), and PU310 (crossed), and the size of the symbol indicates pore size. The inset images are micrographs of the pores at example time points illustrated by arrows in the graphs.

obtained with the PU samples for the projected tissue area plotted as a function of $(t - t_0)$. Altogether 45 data sets are superimposed obtained from 5 experiments with 3 seeding

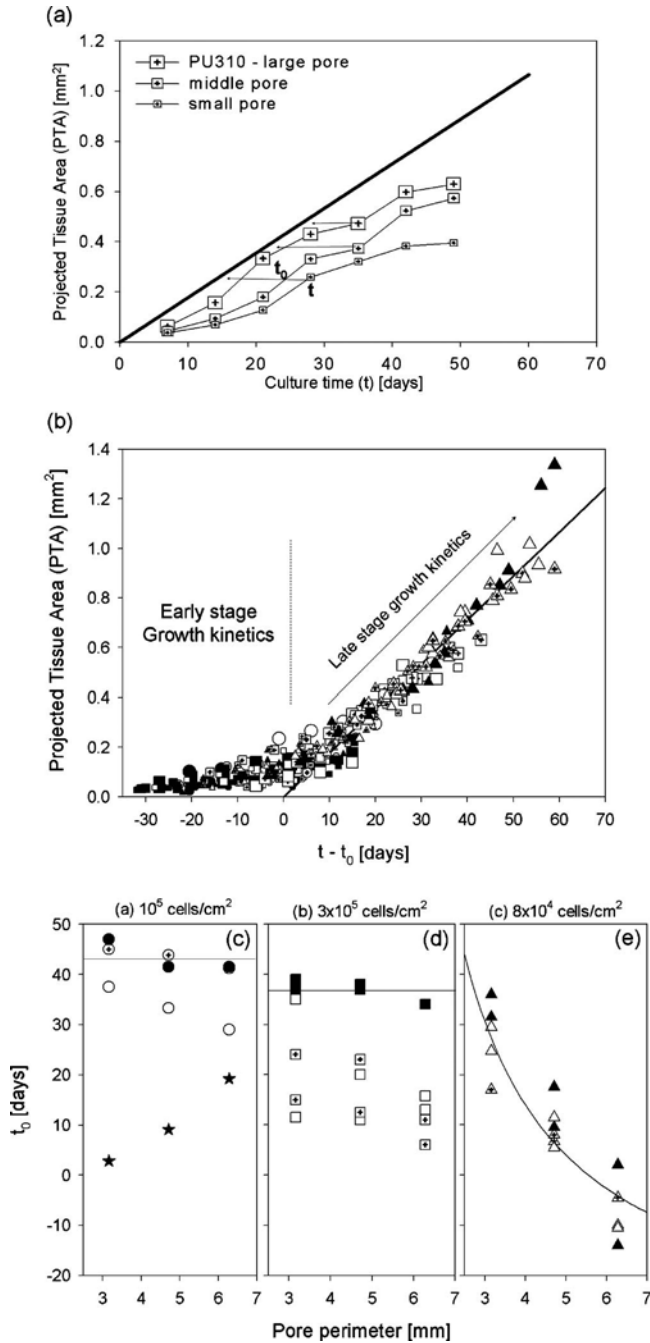


FIG. 5. (a) Description of the delay time (t_0) determination in one of the experiments performed with PU310 with square-shaped pore channels. Projected tissue area was moved horizontally along the X-axis (time) so that they coincide with the data of HA. The shift gives empirically the delay time (t_0). (b) All data from the three different seeding protocols each with three pore sizes and three material types, plotted on top of each other. The full line is the late stage growth kinetics obtained earlier on HA scaffolds. (Symbols represent the different seeding methods: \circ — 10^5 cells/cm², \square — 3×10^5 cells/cm², and \triangle —aspirating cells 8×10^4 cells/cm² into the pores and the black, white, and crossed symbols represent PU75, PU120, and PU310, materials, respectively). The three graphs [(c)–(e)] show the delay time (t_0) for three cell seeding procedures as a function of the pore perimeter. The horizontal lines in (c) and (d) are guides to the eyes, and the line in (e) is the fit of the function $t_0 = a + b/P$. The colors of symbols indicate the type of PU material. The stars in (c) show the values obtained in previous tissue growth experiments on HA for comparison. The values of t_0 significantly vary due to the effect of pore size and seeding method ($P < 0.001$) and there is no difference between PU120 and PU75 (softer material) compared to PU310 (harder material).

procedures, where each experiment had simultaneously 3 pore sizes and 3 materials in the culture medium. Similar data were also found with round pores (data not shown). Figures 5(c)–5(e) give the delay times (t_0) for the three types of seeding procedures, respectively, as a function of the pore size.

IV. DISCUSSION

This article investigates the growth kinetics of three-dimensional tissue formation within the pore channel of polymeric scaffolds made of PU with different stiffnesses. The influence of polymer type and different cell seeding densities on the kinetics of tissue growth within square-shaped pores was observed and compared to a previous study on HA scaffolds.²⁴

The cell culture experiment on these PU scaffolds was carried out using three different cell seeding protocols. The first protocol, being similar to that previously reported on HA scaffolds,²⁴ showed a low proliferation rate of cells on the polymers [Fig. 4(a)]. Therefore, the seeding density was increased in two ways. First, the same protocol was conserved but the cell density was increased by a factor 3. Using this seeding protocol the cells adhere to the surface of the scaffold after seeding. Afterwards cells proliferate and actively migrate into the pores, followed by tissue formation. Second, 8×10^4 cells/cm² were initially dispersed into a small amount of medium and dropped onto the scaffolds. The consequence was that the medium highly enriched with cells was sucked by capillary forces into the pores and cells attach to the inner wall of the pores from the beginning.

During the initial period of cell culture on the surface of the scaffold, fewer cells were observed on PU120 and PU75 compared to PU310. This suggests that substrate stiffness has an impact on cell adhesion and cell spreading [Figs. 2(a) and 2(b)]. As substrate stiffness was modulated by varying the H₁₂MDI/1,4-BD to H₁₂MDI/PTMEG segment ratio, it cannot be ruled out that small changes in chemistry are responsible for the different cell responses. Furthermore, differentiation of osteoblast precursor cells seems to be accelerated by a stiffer substrate, as observed in the case of PU310 [Fig. 2(c)]. This is consistent with the known influence of substrate stiffness on cell behavior and differentiation known from other cell types.^{12–14} Of course surface roughness could also influence cell adhesion and spreading; however, the differences observed do not correlate with the cell culture observations.

Cells seeded on the scaffolds adhered initially to the surface of the pore channel, then started to proliferate, and produce extracellular matrix forming a tissue layer. Cells at the corner of the square pores showed higher proliferation rates and by this behavior formed a network leaving a round central canal open, regardless of the original pore shape. As seen in the previous study,²⁴ similar growth kinetics were observed with both round and square pores with the same initial perimeter (data not shown). With increasing culture time, this round inner boundary decreased in diameter, but kept its

shape until complete closure resembling the fourth stage of new tissue formation by osteoblastlike cells described as an “osteonlike” structure by Frosch *et al.*³⁹

Several remarkable observations can be made based on Fig. 5.

- (1) The raw data [Figs. 4(a)–4(c)] obtained from the microscopy observations during the culture period agree remarkably well after the time scales are shifted by an empirical delay time t_0 [Fig. 5(a)].
- (2) The late stage growth is linear and the slope agrees perfectly with what was found for tissue growth on HA. This slope is independent of the seeding procedure and of the material, indicating that the late stage tissue growth kinetics is universal for the type of cells considered [Fig. 5(b)].
- (3) The delay time before this universal growth behavior is reached can be substantial (in the order of 1 month) and varies strongly with material type and with cell seeding density.
- (4) For all PU materials, the delay time (at similar cell seeding conditions) is larger than for HA [Fig. 5(c)].
- (5) There are only small differences between the PU materials. Only the softest material PU75 displays a somewhat longer delay time (full symbols), this is seen for all cell seeding densities.
- (6) The cell seeding density has a dramatic effect on the delay time before the onset of universal three-dimensional growth. Indeed, at normal seeding densities, the delay time only slightly increases with pore perimeter [Fig. 5(c)], at higher densities there is virtually no dependence on pore perimeter [Fig. 5(d)], and when the cells are sucked directly into the pores the delay time decreases substantially with pore perimeter [Fig. 5(e)].

The progression of new tissue formation shows a time dependent development and follows two main steps, which can be described as an early and a late stage in growth. First, cell-material interactions play a crucial role at the very beginning and determine cell attachment and proliferation. This is seen clearly in the strong dependence of the delay time t_0 on the type of material with the delay time being longer for tissue growth on PU than on HA. This difference can amount to several weeks, which is crucial from a tissue engineering point of view. The critical initial step, cell attachment to the scaffold, involves the formation of focal adhesions, those mediate cell anchoring by physically coupling integrin receptors to the contractile actin cytoskeleton. The pattern of focal adhesions expressed is highly dependent on surface properties, such as chemistry and topographical features.^{17,20,40} HA and PU materials provide differences in surface chemistry. This may result in the creation of different focal adhesion molecules. It is known that patterns of vinculin and focal adhesion kinase expression differ strongly when osteoblasts are seeded either onto HA or onto titanium or glass surfaces.^{41,42} We speculate that cell adhesion is more efficient on HA than on PU, which gives a higher initial cell number on HA after seeding, confluence is reached sooner, and multilayer tissue formation starts earlier in HA.

Cells were seeded using three protocols allowing for the formation of a confluent cell layer in 1 to 3 days. The cell seeding density has a dramatic effect on the delay time. This is not unexpected as the cell seeding density influences the time until a confluent cell layer is formed on top of the material and growth into the third dimension can start.⁴³ With the lowest cell seeding density, cells need time to proliferate before they can migrate from the flat substrate surface into the pores perpendicular to it. When the cell seeding density is increased by threefold, cells take a very short time to reach confluence and the migration can start much earlier resulting in little dependence of the delay time on pore perimeter [Fig. 5(d)]. Once cells are confluent on the outer surface then the number of cells available to move into the pore will be proportional to the pore perimeter (i.e., $\sim 4a$, where a is the side length of the square cross section of the pore). The surface area inside the pore that will be covered by cells migrating from the boundary is also proportional to the pore perimeter ($\sim 4ad$, where d is the pore depth). This means that the expected time for cells to become confluent within the pore will be independent of the perimeter, consistent with Figs. 5(c) and 5(d). When a concentrated cell suspension is sucked into the pores [as for Fig. 5(e)], many more cells end up in larger pores than in smaller ones. In fact, the number of cells in a pore will scale with the square of its side length, while the surface to be covered within the pore remains proportional to the perimeter ($\sim 4ad$). This would suggest that the delay time would scale inversely with pore size. The data in Fig. 5(e) are fitted well with such an inverse relation providing qualitative support for this hypothesis.

In late stages of tissue formation by the osteoblastlike cells, attachment and proliferation were followed by the autonomous synthesis of a collagen matrix. Once sufficient tissue is formed cell-scaffold interactions become irrelevant and the multilayer network of the extracellular matrix (ECM) overtakes the part of the scaffold material as the main controller of cell response. Ongoing three-dimensional amplification of the new tissue now follows new rules and boundary conditions, namely, pliability of the extra cellular matrix, the development of forces within the matrix, and the local geometry (curvature) of the tissue surface itself.^{24,44} The late stage growth kinetics in the PU scaffolds were observed to be exactly the same as that of HA, and the growth kinetics is again consistent with a growth law in which the local growth rate is proportional to the local curvature of the tissue layer previously produced by the cells, as shown in HA.²⁴ The fact that the slope of the late growth curve does not depend on cell seeding density or on the type of material and is even the same for polymer and HA (observations 1 and 2) indicates that at these late stages of tissue growth the supporting material plays a little role. At this stage, the extracellular tissue layer is thick enough to support the cells independent of the scaffold and the growth kinetics depends only on the interaction between the cells and their own ECM. This is not unexpected but demonstrates the importance of the millimeter-size architecture of the scaffold because this is

what determines the shape of the tissue layer and, hence, the late stage growth kinetics. In summary, the architecture of the scaffold is more important than its chemical nature for supporting the late stages of tissue growth.

V. CONCLUSIONS

In this article, a model scaffold with square pore channels made of PU with different stiffnesses (in the megapascal range) was used to investigate the tissue formation by osteoblast cells inside the channels. We showed that three-dimensional tissue growth by MC3T3-E1 preosteoblast cells in the polymer scaffolds can be roughly divided into two stages. In the early stage, cells form a confluent layer on top of the scaffold where cell-material interactions, such as cell adhesion, which is dependent on the stiffness of the three-dimensional scaffolds and inner surface roughness of the pores, have a strong influence on the growth kinetics. In the late stage, cells grow within their own matrix and further three-dimensional tissue amplification depends only on geometry but not on the scaffold material. A universal growth law identical to what was found on HA scaffolds was found, which depends on scaffold architecture only. The delay time (t_0) to reach the late stage is strongly dependent on the seeding protocol and can become so long (month or longer) in unfavorable cases that the system never reaches the late stage of three-dimensional growth. This systematic analysis provides insights into how geometric constraints may guide tissue formation *in vitro* and shows that optimizing scaffold architectures may improve tissue formation independently of the scaffold material.

ACKNOWLEDGMENTS

The authors are grateful to Deutsche Forschungsgemeinschaft (DFG) for financial support under grant of collaborative research center scheme (SFB) Grant No. 760, part Project B3.

¹D. W. Hutmacher, *J. Biomater. Sci., Polym. Ed.* **12**, 107 (2001).

²R. Langer, L. G. Cima, J. A. Tamada, and E. Wintermantel, *Biomaterials* **11**, 738 (1990).

³A. S. P. Lin, T. H. Barrows, S. H. Cartmell, and R. E. Guldberg, *Biomaterials* **24**, 481 (2003).

⁴T. M. G. Chu, D. G. Orton, S. J. Hollister, S. E. Feinberg, and J. W. Halloran, *Biomaterials* **23**, 1283 (2002).

⁵D. G. Castner and B. D. Ratner, *Surf. Sci.* **500**, 28 (2002).

⁶N. Faucheux, R. Schweiss, K. Lutzow, C. Werner, and T. Groth, *Biomaterials* **25**, 2721 (2004).

⁷A. S. G. Curtis and C. D. Wilkinson, *J. Biomater. Sci., Polym. Ed.* **9**, 1313 (1998).

⁸J. Park, S. Bauer, K. A. Schlegel, F. W. Neukam, K. von der Mark, P. Schmuki, *Small* **5**, 666 (2009).

⁹O. Zinger, G. Zhao, Z. Schwartz, J. Simpson, M. Wieland, D. Landolt, and B. Boyan, *Biomaterials* **26**, 1837 (2005).

¹⁰B. D. Boyan, V. L. Sylvia, Y. H. Liu, R. Sagun, D. L. Cochran, C. H. Lohmann, D. D. Dean, and Z. Schwartz, *Biomaterials* **20**, 2305 (1999).

¹¹P. Linez-Bataillon, F. Monchau, M. Bigerelle, and H. F. Hildebrand, *Bio-*

mol. Eng. **19**, 133 (2002).

¹²D. E. Discher, P. Janmey, and Y. L. Wang, *Science* **310**, 1139 (2005).

¹³H. J. Kong, T. R. Polte, E. Alsberg, and D. J. Mooney, *Proc. Natl. Acad. Sci. U.S.A.* **102**, 4300 (2005).

¹⁴C. M. Lo, H. B. Wang, M. Dembo, and Yu-li Wang, *Biophys. J.* **79**, 144 (2000).

¹⁵A. J. Engler, S. Sen, H. L. Sweeney, and D. E. Discher, *Cell* **126**, 677 (2006).

¹⁶K. Anselme, M. Bigerelle, B. Noel, E. Deufresne, D. Judas, A. Iost, and P. Hardouin, *J. Biomed. Mater. Res.* **49**, 155 (2000).

¹⁷C. S. Chen, M. Mrksich, S. Huang, G. M. Whitesides, and D. E. Ingber, *Science* **276**, 1425 (1997).

¹⁸S. V. Graeter, J. H. Huang, N. Perschmann, M. López-García, H. Kessler, J. Ding, and J. P. Spatz, *Nano Lett.* **7**, 1413 (2007).

¹⁹J. Park, S. Bauer, K. von der Mark, and P. Schmuki, *Nano Lett.* **7**, 1686 (2007).

²⁰J. P. Spatz and B. Geiger, in *Cell Mechanics—Methods in Cell Biology*, edited by Y. L. Wang and D. E. Discher (Elsevier, New York, 2007), Vol. 83, pp. 89.

²¹F. J. O'Brien, B. A. Harley, I. V. Yannas, and L. J. Gibson, *Biomaterials* **26**, 433 (2005).

²²E. Charrière, J. Lemaitre, and Ph. Zysset, *Biomaterials* **24**, 809 (2003).

²³J. Zeltinger, J. K. Sherwood, D. A. Graham, R. Müeller, and L. G. Griffith, *Tissue Eng.* **7**, 557 (2001).

²⁴M. Rumpler, A. Woesz, J. W. C. Dunlop, J. T. van Dongen, P. Fratzl, *J. R. Soc., Interface* **5**, 1173 (2008).

²⁵J. E. Davies, *Anat. Rec.* **245**, 426 (1996).

²⁶T. A. Owen, M. Aronow, V. Shalhoub, L. M. Barone, L. Wilming, M. S. Tassinari, M. B. Kennedy, S. Pockwinse, J. B. Lian, and G. S. Stein, *J. Cell. Physiol.* **143**, 420 (1990).

²⁷V. Thomas, T. V. Kumari, and M. Jayabalan, *Biomacromolecules* **2**, 588 (2001).

²⁸K. P. Kommareddy, C. Lange, M. Rumpler, M. Inderchand, J. Cui, K. Kratz, J. H. Börgermann, A. Lendlein, P. Knaus, and P. Fratzl, *Bone* **44**, S261 (2009).

²⁹N. M. K. Lamba, K. A. Woodhouse, and S. L. Cooper, *Polyurethanes in Biomedical Applications* (CRC, Boca Raton, FL, 1998), 277 pp.

³⁰H. John Crabtree, *ASAIO J.* **49**, 290 (2003).

³¹J. Cui, K. Kratz, and A. Lendlein, *Mater. Res. Soc. Symp. Proc.* **1190**, 93 (2009).

³²R. Mohr, K. Kratz, T. Weigel, M. Lucka-Gabor, M. Moneke, and A. Lendlein, *Proc. Natl. Acad. Sci. U.S.A.* **103**, 3540 (2006).

³³J. Cui, K. Kratz, and A. Lendlein, *Smart Mater. Struct.* **19**, 065019 (2010).

³⁴J. Cui, K. Kratz, M. Heuchel, B. Hiebl, and A. Lendlein, *Polym. Adv. Technol.* (in press).

³⁵L. D. Quarles, D. A. Yohay, L. W. Lever, R. Caton, R. J. Wenstrup, *J. Bone Miner. Res.* **7**, 683 (1992).

³⁶J. Y. Choi, B. H. Lee, K. B. Song, R.-W. Park, I.-S. Kim, K.-Y. Sohn, J.-S. Jo, and H.-M. Ryoo, *J. Cell. Biochem.* **61**, 609 (1996).

³⁷M. Rumpler, A. Woesz, F. Varga, I. Manjubala, K. Klaushofer, and P. Fratzl, *J. Biomed. Mater. Res. Part A* **81A**, 40 (2007).

³⁸N. Fratzl-Zelman, H. Hörandner, E. Luegmayr, F. Varga, A. Ellinger, M. P. M. Erlee, and K. Klaushofer, *Bone* **20**, 225 (1997).

³⁹K. H. Frosch, F. Barvencik, C. H. Lohmann, V. Viereck, H. Siggelkow, J. Breme, K. Dresing, and K. M. Stürmer, *Cells Tissues Organs* **170**, 214 (2002).

⁴⁰V. G. Brunton, I. R. J. MacPherson, and M. C. Frame, *Biochim. Biophys. Acta* **1692**, 121 (2004).

⁴¹A. Okumura, M. Goto, T. Goto, M. Yoshinari, S. Masuko, T. Katsuki, and T. Tanaka, *Biomaterials* **22**, 2263 (2001).

⁴²M. A. Woodruff, P. Jones, D. Farrar, D. M. Grant, and C. A. Scotchford, *J. Mol. Histol.* **38**, 491 (2007).

⁴³G. Cheng, B. B. Youssef, P. Markenscoff, and K. Zygorakis, *Biophys. J.* **90**, 713 (2006).

⁴⁴B. Geiger, *Science* **294**, 1661 (2001).